Carbohydrate Polymer Technologies and Applications 13 (2026) 101103

Contents lists available at ScienceDirect

Carbohydrate Polymer Technologies and Applications

journal homepage: www.sciencedirect.com/journal/carbohydrate-polymer-technologies-and-applications

Design of responsive films using phenylurea modified chitosan and *Viburnum tinus* L. extract as natural indicator

Mouad El Mouzahim [a], Alessandro Pedrini [a], Enrico Dalcanale [a], N. Riboni [a], F. Bianchi [a], A. Jorge Parola [b], Roberta Pinalli [a,1,*]

[a] Department of Chemistry, Life Sciences and Environmental Sustainability, University of Parma, INSTM, UdR Parma, Parco Area delle Scienze 17/A, Parma 43124, Italy

[b] LAQV-REQUIMTE, Department of Chemistry, NOVA School of Science and Technology, NOVA University Lisbon, 2829-516 Caparica, Portugal

ARTICLE INFO

Keywords:
Chitosan
Phenylurea
Viburnum tinus L.
Multiple hydrogen bonding
UV barrier

ABSTRACT

Chitosan (Cs) films are attractive for sustainable packaging due to biodegradability and intrinsic antimicrobial activity, yet their barrier and mechanical performances are often insufficient for demanding applications. Here, we report a two-step strategy combining covalent phenylurea grafting on chitosan (Cs-PU) with the incorporation of a *Viburnum tinus* L. fruit ethanolic extract (VTE) as a natural, pH-responsive indicator. Phenylurea grafting was designed to introduce strong, directional intermolecular interactions within the polymer matrix and led to marked improvements in film performance: compared with pristine Cs, Cs-PU showed ~25 % higher tensile strength, a higher surface hydrophobicity (water contact angle: 81.8° → 101.2°), and a lower water vapor permeability (3.5 → 2.6 × 10^{-11} g·m^{-1}·s^{-1}·Pa^{-1}). VTE, not previously reported as an additive for biopolymer film modification, endowed the films with pH-responsive optical functionality, producing a clear and reversible color shift over pH 0–14, while maintaining good structural and barrier properties. As a proof-of-concept application, Cs-PU@VTE films were used as headspace indicator labels for Atlantic cod (Gadus morhua): the labels exhibited rapid and sensitive colorimetric responses to spoilage-related volatile amines, with visible changes within 24 h at room temperature, enabling real-time freshness monitoring. Overall, this work demonstrates an integrated approach to obtain bio-based films that combine improved mechanical/barrier properties with smart colorimetric functionality for potential packaging applications.

1. Introduction

Chitosan, a biopolymer derived from chitin, is a promising candidate for sustainable food packaging due to its biodegradability, biocompatibility, and intrinsic antimicrobial and antioxidant properties. (Haghighi et al., 2020; Han et al., 2018; Oladzadabbasabadi et al., 2022; Sid et al., 2021). However, to enable its use in demanding applications, its limited mechanical strength and barrier properties often necessitate enhancement (Cazón & Vázquez, 2020; Juikar & Warkar, 2023; Peh et al., 2000). Researchers have extensively explored chemical modification as a primary strategy to improve these features. Techniques like grafting or cross-linking are widely used to create a more robust film structure. Grafting involves attaching new small molecules or polymer chains to the chitosan backbone (Kumar et al., 2020; Thakur & Thakur, 2014), while cross-linking creates a three-dimensional network by forming covalent or ionic bonds between chitosan molecules, both of which significantly enhance mechanical integrity (Berger et al., 2004). In addition to these structural improvements, the incorporation of natural additives like plant extracts and essential oils has contributed to developing "smart" and active packaging (Frank et al., 2018; Hossain et al., 2019; Koosha & Hamedi, 2019; Rojas-Bravo et al., 2019; Shankar et al., 2021; Sutharsan et al., 2022; W. Zhang & Jiang, 2020). These additives can introduce new functionalities, such as antioxidant and pH-sensitive properties, which are often lacking in the modified chitosan itself. For example, some plant extracts contain anthocyanins that change color with pH, enabling the films to function as visual freshness indicators (Amaregouda et al., 2022; Chen et al., 2020; Gasti et al., 2021). This dual approach of chemical modification for structural enhancement and natural additives incorporation for intelligent functionality is key to developing next-generation food packaging materials.

* Corresponding author.
E-mail address: roberta.pinalli@unipr.it (R. Pinalli).
[1] Scopus Author ID: 6506474623

https://doi.org/10.1016/j.carpta.2026.101103

Available online 13 February 2026

In this context, some studies have already reported two-step strategies for chitosan-based films, typically involving an initial chemical or physical modification of the polymer matrix followed by the incorporation of bioactive natural compounds. For instance, chitosan or chitosan-based blends have been crosslinked using natural or synthetic agents (e.g., genipin, citric acid, or PEG-based crosslinkers) prior to loading essential oils, polyphenols, or other plant-derived extracts to impart antioxidant and antimicrobial activity (Choo et al., 2021; Roy & Rhim, 2022; Stefanowska et al., 2023; Yang et al., 2024). These approaches have demonstrated that sequential modification can successfully enhance either structural properties or bioactivity, and in some cases both. However, in most reported systems, the first modification step primarily serves as a generic stabilization or crosslinking strategy, while the second step focuses on introducing bioactivity, with limited emphasis on designing specific supramolecular interactions to synergistically reinforce mechanical performance and functional responsiveness.

We present the chemical modification of chitosan through the introduction of phenyl urea groups as a powerful approach for improving film properties, particularly mechanical strength and water vapor barrier performance, which represent key limitations of native chitosan films in packaging applications. This modification is designed to maximize the formation of hydrogen bonds within the polymer matrix (Hamann et al., 2001; Wu et al., 2023). These bonds will act as strong intermolecular forces, leading to a denser and more rigid material, thereby reducing water vapor permeability through the film and enhancing its tensile strength.

Additionally, we add to the matrix *Viburnum tinus* L. fruit extract, a natural additive rich in flavonoids and phenolic compounds (Cometa et al., 1998; Mohamed et al., 2005). These have well known antioxidant properties, which are critical for protecting packaged food from oxidative damage and extending its shelf life. More specifically, the extract contains anthocyanin dyes, which are key to its dual functionality (Jordheim et al., 2007). These natural dyes undergo reversible structural transformations in response to changes in pH, leading to a visible color shift (Fig. 1) (Pina et al., 2012; Roy & Rhim, 2021). This distinctive attribute allows the film to function as a visual freshness indicator, changing color in response to spoilage-related pH shifts, such as the release of basic volatile amines from decaying food (Chen et al., 2020; Kurek et al., 2019; Qin et al., 2024; Yong et al., 2019).

The present work introduces a phenyl urea grafting motif specifically designed to promote strong, directional hydrogen bonding within the chitosan matrix, followed by the incorporation of a previously unexplored *Viburnum tinus* L. fruit extract. The coupling of a H-bonded reinforced polymer network with a pH-responsive natural extract enables the simultaneous enhancement of mechanical strength, water and UV barrier properties, and intelligent colorimetric functionality.

2. Material and methods

2.1. Materials

Chitosan (Cs, purity 85–90 %, degree of deacetylation ≥ 80 %, molecular weight 10–15 kDa, viscosity 20–100 mPa·s in 0.5 % acetic acid at 20 °C) and hexamethylene diisocyanate (HDI, ≥98 % purity) were purchased from TCI (USA). Glacial acetic acid (purity ≥99.7 %), 1,1-diphenyl-2-picrylhydrazyl (DPPH, purity ≥95 %), folin & ciocalteu reagent (quality level 200, concentration 2 N), dibutyltin dilaurate (DBTL, purity ≥95 %), aniline (purity ≥99 %), gallic acid(purity ≥99 %), were obtained from Sigma-Aldrich (USA). All reagents and solvents were of analytical grade and were used without further purification.

2.2. Preparation of 1-(5-isocyanatopentyl)-3-phenylurea (PU isocyanate)

Aniline was subjected to a reaction with an excess of hexamethylene diisocyanate (9 equivalents) within an inert atmosphere, at room temperature for 4 h (**Fig. S1**). The reaction was quenched by adding cyclohexane; the resulting precipitate was filtered and washed with cyclohexane to remove unreacted HDI (Yield = 82 %). The resulting white solid was dried under vacuum and characterized by ^{1}H NMR (400 MHz, DMSO-d_6): δ ppm 8.35 (s, 1H), 7.34 (dd, 2H), 7.20 (t, 2H), 6.87 (t, 1H), 6.10 (t, 1H), 3.07 (q, 2H), 1.61 – 1.49 (m, 2H), 1.42 (s, 2H), 1.37 – 1.22 (m, 6H) (**Fig. S1**).

2.3. Preparation of Cs-PU

5 g of chitosan powder was suspended in 50 mL dry DMSO, followed by the addition of 3 drops of dibutyltin dilaurate (DBTL) and 160 mg of PU isocyanate, which represents 2.5 mol % of the deacetylated monomers. The polymer suspension was reacted for 4 h then the modified polymer was recovered by filtration, washed by DMSO to remove unreacted isocyanate then dried under vacuum at 80 °C. To assess grafting efficiency, UV calibration curves of PU in DMSO were established and employed to quantify the unreacted fractions recovered during the washing steps (**Fig. S3**).The PU isocyanate grafting was confirmed via FT-IR (**Fig. S4**).

2.4. Preparation of VTE

Ripe fruits of *Viburnum tinus L.* were provided by the botanic garden of NOVA FCT (Lisbon, Portugal). The fruits were thoroughly washed

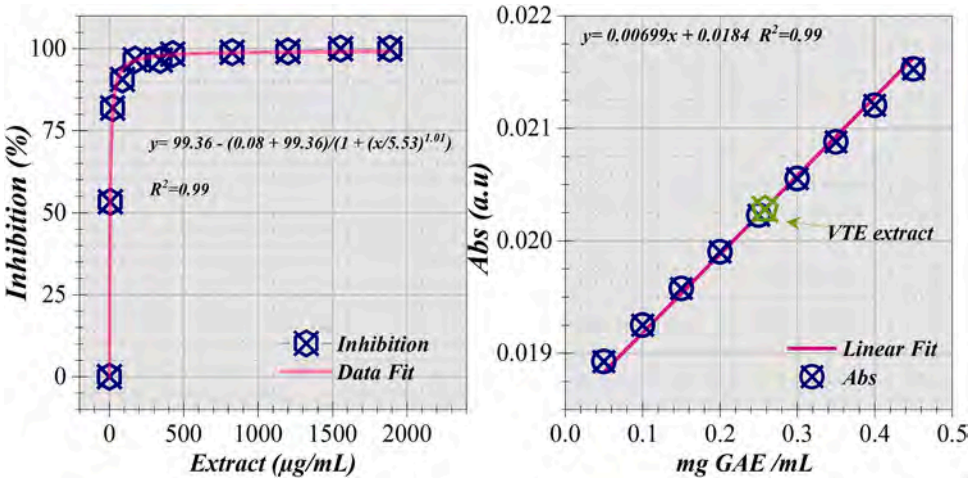

Fig. 1. DPPH scavenging (A) and total phenol content (B) analysis of VTE.

with distilled water when received to eliminate impurities. The cleaned fruits were then air-dried at room temperature and then subjected to maceration using a 90 % ethanol solution, with a solid-to-solvent ratio of 1:10 (w/v). The maceration process was carried out at room temperature for 24 h under agitation to enhance the diffusion of bioactive compounds into the solvent. After the extraction period, the mixture was filtered to remove solid residues, and the resulting filtrate was concentrated under reduced pressure using a rotary evaporator at 40 °C. This process yielded a viscous dark extract, referred to as *Viburnum tinus* L. extract (VTE), with an average extraction yield ranging from 10 % to 15 % (w/w) based on the initial mass of fresh fruits. Residual solvents were analyzed by headspace gas chromatography-mass spectrometry (HS GC–MS) in accordance with ICH Q3C (R9). The extract was stored in amber glass containers at 4 °C for further use and characterization in terms of phenolic content, antioxidant activity, and anthocyanin reactivity to pH.

2.5. Films preparation

The polymeric films were prepared by dissolving 1 % w/v of the polymer (Cs pristine and Cs-PU) in aqueous acetic acid solution (1 % v/v) and stirring at room temperature until Cs completely dissolved. Cs and the Cs-PU films were obtained via solution casting in polystyrene petri dishes. The film was dried at 40 °C for 48 h. To prepare the Cs-PU@VTEs films, 150 μL, 250 μL and 500 μL of a 13.3 mg/mL VTE ethanolic aqueous solution (8:2 ethanol/water) were added separately to the Cs-PU polymeric solution to obtain films with different composition as listed in **Table S2**. The resulting films were designated as Cs-PU@VTE150, Cs-PU@VTE250, and Cs-PU@VTE500, respectively.

2.6. VTE characterization

2.6.1. Phenolic content

The total phenolic content (TPC) of VTE was determined using the Folin–Ciocalteu colorimetric method (Siddiqui et al., 2017), with gallic acid as the standard. Briefly, 1 mL of the extract (1 g/100 mL of ethanol) was mixed with 5 mL of Folin–Ciocalteu reagent (previously diluted 10-fold with distilled water). After 5 min of incubation at room temperature, 4 mL of 7 % (w/v) sodium carbonate (Na_2CO_3) solution was added to the mixture. The reaction was allowed to proceed for 30 min in the dark at room temperature. The absorbance of the resulting blue color was measured at 765 nm using a UV–Vis spectrophotometer against a reagent blank. A calibration curve was established using gallic acid solutions at known concentrations. TPC value was calculated using the following Eq. (1):

$$TPC\ mg_{GAE}\Big/g_{Dry\ sample} = \frac{C_{GAE}}{C_{\ extract}} \tag{1}$$

where C_{GAE} represents the concentration of gallic acid equivalents in VTE sample solution (in mg/mL), calculated from the calibration curve, and $C_{\ extract}$ represents the concentration of the dry extract in the reaction solution prepared as previously mentioned (0.001 g/mL).

2.6.2. Antioxidant activity

The antioxidant activity of VTE was evaluated using DPPH radical scavenging assays (Jiang et al., 2023). A 0.1 mM solution of DPPH in methanol was prepared, and different aliquots (μL) of a 15 μg/μL extract solution were mixed with 3 mL of this solution. The mixture was incubated in the dark at room temperature for 30 min, after which the absorbance was measured at 517 nm. The inhibition percentage of radicals was calculated using the formula on Eq. (2):

$$\%Inhibition = \frac{(A_0 - A_S) \times 100}{A_S} \tag{2}$$

where A_0 is the absorbance of the control and A_s is the absorbance in presence of the extract. The IC_{50} values, indicating the concentration required to scavenge 50 % of the radicals, were determined from the inhibition curves. All measurements were performed in triplicate, with ascorbic acid used as a reference standard.

2.6.3. Anthocyanin pH-sensitivity

A solution of anthocyanin was prepared by dissolving 2 mg of the VTE in 3 mL of phosphate buffer (0.1 M, prepared from NaH_2PO_4/Na_2HPO_4, pH 7.0) then the pH was adjusted using 1 M HCl and NaOH solutions. The buffers used covered a pH range typically from 0 to 14 to observe the colorimetric response of anthocyanin under different pH environments. After complete dissolution, the solutions were allowed to equilibrate at room temperature for 30 min in the dark to prevent photodegradation. The changes in color were recorded visually and by measuring the absorbance spectra using a UV–Vis spectrophotometer over the wavelength range of 400–700 nm.

2.7. Films characterization

2.7.1. Thickness, color, and UV barrier properties

The thickness of the film was measured using a digital micrometer provided by Wenzhou Sanhe Measuring Instrument Co., Ltd. (Zhejiang, China), with an accuracy of 1 μm. Simultaneously, color characteristics, including *L*, *a*, and *b* that represent respectively the brightness, red-green, and yellow-blue, were acquired in reflective mode by utilizing an integrating sphere in conjunction with Jasco spectra manager software, employing the Jasco V-670 from Jasco Ltd. (Japan). The overall color difference (ΔE), as well as the whiteness index (WI) and yellowness index (YI), were computed utilizing the subsequent formulas (Liu et al., 2017).

$$\Delta E = \sqrt{(L^* - L)^2 + (a^* - a)^2 + (b^* - b)^2} \tag{3}$$

$$WI = 100 - \sqrt{(100 - L)^2 + a^2 + b^2} \tag{4}$$

$$YI = 142.86 \times \left(\frac{b}{L}\right) \tag{5}$$

The values $L^* = 87.97$, $a^* = 0.36$, and $b^* = 1.64$, represent the color parameters of a standard plate with a white color that served as reference values, while *L*, *a*, and *b* represented the color parameter values of the film sample.

To evaluate the UV–visible light-blocking abilities of the films, we performed light transmission measurements in transmission mode using a solid sample holder with the Jasco V-670 UV–vis spectrophotometer.

2.7.2. Moisture content, water vapor permeability and water contact angle

Moisture content determination for the films involved a gravimetric method, wherein the film samples were subjected to drying at 100 °C until a consistent weight was attained, followed by the application of Eq. (6) (X. Zhang et al., 2019):

$$Moisture\ content(\%) = \frac{(W_f - W_0)}{W_0} \times 100 \tag{6}$$

In this context, W_f (g) represents the sample weight subsequent to the drying procedure, while W_0 (g) corresponds to the initial dry weight of the sample.

The water vapor permeability (WVP) tests were carried out utilizing the method reported by Liu et al. (2017) and X. Zhang et al. (2019) with some adjustments. To begin, the film specimens were hermetically affixed to the top of a 15-mL centrifuge tube, effectively employing the film as a lid for the tube. These tubes were filled with calcium chloride and placed in a desiccator at room temperature, alongside a beaker containing purified water. Following a 24-hour duration, the films were weighed, and the calculation of water vapor permeability (WVP) was

executed using Eq. (7):

$$WVP\ \left(g.m^{-1}.s^{-1}.Pa^{-1}\right) = \frac{W \times e}{t \times A \times \ \Delta P} \quad (7)$$

where, W (g) refers to the augmented mass of the centrifuge tube, e (m) is the depth of the film, t (s) represents the duration of the test, A (m^2) is the surface area of the film sample, and ΔP (Pa) refers to the water vapor partial pressure (in Pascals) at a temperature of 20 °C.

Water contact angle (WCA) values of each film were measured using a Biolin Scientific Attension Theta Flex goniometer. A 4 μL droplet of distilled water was placed on three separate spots on each film, and the contact angles were recorded with a high-speed digital camera.

2.7.3. Mechanical properties

The tensile strength, strain at the break, and Young's modulus of the films were measured using an Lr 50 K plus, Llyod material tester (AMETEK (STC)., BR, UK) with an initial grip distance of 3.5 cm and a crosshead speed of 3 mm/min Liu et al. (2017). A 6 cm × 1 cm film sample was utilized for the test.

2.7.4. Scanning electron microscopy (SEM)

A Quanta FEG 250 electron microscope (Thermo Fisher Scientific, USA) was used to analyze the surface morphology and cross-section of the film at an accelerating voltage of 5 kV. Metal stubs with double-adhesive carbon tape were used to mount the film samples. A conductive layer of gold was coated on the samples, and SEM images were taken at 400 and 850 magnifications.

2.7.5. Fourier transform infrared analysis

Fourier transform infrared spectrum (FTIR) of the films was recorded using a PerkinElmer FT-IR Spectrum Two spectrometer in Attenuated Total Reflectance (ATR) detection mode. This was performed over spectral ranges of 4000–400 cm^{-1}, employing a resolution of 4 cm^{-1} and an average of 32 scans per sample. Then, the background spectra were subtracted from all measurements.

2.7.6. Thermal stability

Thermogravimetric analysis (TGA) was performed was performed using a Perkin Elmer TGA 8000 equipped with a GC10 gas controller (pure air/nitrogen), Mettler Toledo at a rate of 10 °C/min in air.

2.7.7. Antioxidant activity

The antioxidant properties of the films were evaluated using the DPPH radical scavenging assay, as described by Wang et al. (2019). Film samples with a diameter of 0.5 cm and with the same weight were treated with 4 ml of a $-1.0\ 10^{-4}$ M methanolic DPPH solution at ambient conditions and in the dark for 1 h. The absorbance of the solution at 517 nm was measured, and Eq. (8) was used to calculate the antioxidant activity:

$$\text{DPPH radical scavenging activity}\ (\%) = \frac{(A_0 - A_1)}{A_0} \times\ 100 \quad (8)$$

Where A_0 and A_1 were the absorbances of the blank and reaction solution, respectively.

2.7.8. pH-sensitivity of films

To monitor the color change of the films exposed to different pH levels, acidic (HCl) and alkaline (NaOH) solutions were prepared. The anthocyanin-containing film was soaked in the prepared acidic or alkaline solutions for 2 min, and color change was monitored.

2.7.9. Ammonia-sensitivity of films

Ammonia-sensitivity was determined by placing the film (2 cm × 2 cm) in a petri dish suspended 5 cm above a 0.1 M ammonia solution (15 mL) in a closed container. The color parameters of the films were recorded after 10, 20, and 30 min of exposure.

2.7.10. Food freshness monitoring

To evaluate fish freshness, Cs-PU@VTE films were employed as indicator labels. Specimens of Atlantic cod (*Gadus morhua*) were placed in transparent containers, with the labels affixed to the inner headspace. The containers were hermetically sealed and incubated at 25 ± 1 °C for three days. To monitor freshness, color transitions were documented daily via photography, and the CIELAB color parameters (***L, a***, and ***b***) were quantitatively recorded.

2.8. Statistical analysis

Data for each test were statistically analyzed using ORIGIN LAB 8.5 software. One-way ANOVA test was used to evaluate the significance of the difference between factors and levels. A comparison of means was conducted using a Tukey test at $p < 0.05$. All treatments were triplicated and data were presented as mean ± SD.

3. Result and discussion

3.1. VTE characteristics

The total phenolic content (TPC) of VTE was analyzed via Folin–Ciocalteu colorimetric method and resulted to be 258.2 mg GAE/g dry weight (Fig. 1B and Eq. (1)), indicating a rich diversity of phenolic compounds with considerable antioxidant potential. This was confirmed by its strong performance in the DPPH assay (IC_{50} = 5.54 μg/mL, Fig. 1), demonstrating a high capacity to neutralize free radicals. These results are in close agreement with the literature (Sever Yilmaz et al., 2013), where it is reported that *V. tinus* fruit methanol extracts, characterized by high phenolic and flavonoid contents, displayed exceptional activity across multiple antioxidant assays (DPPH, DMPD, nitric oxide scavenging, and FRAP), ranking among the most potent antioxidants in the genus.

In aqueous solution, the VTE exhibits a color change as a function of pH (Fig. 2), a behavior characteristic of anthocyanin-containing systems. At low pH (0–3), the extract appears red, corresponding to the flavylium cation form (see Fig. 3 built bas), which absorbs strongly in the UV and blue–green visible regions. As the pH increases, this red coloration fades due to the formation of colorless or weakly absorbing hemiketal and chalcone species (Fig. 3). Under basic conditions (pH > 10), the solution develops a green hue within the first minute, indicative of anionic quinoidal bases (Fig. 1); this color gradually shifts to deep orange over time. Such pH-dependent chromatic transitions are fully consistent with the anthocyanin composition reported for Viburnum species (Jordheim et al., 2007), where cyanidin 3-glycoside and 3, 5-diglycosides, often with sugar moieties such as glucose or xylose, were identified as the predominant dyes. These structural variations influence the electronic properties and stability of the chromophores, thereby modulating their visible color in response to proto-nation–deprotonation equilibria. Furthermore, the additional UV absorbance observed below 400 nm under all the pH conditions suggests the presence of co-extracted phenolic compounds, which may further influence certain anthocyanin forms and contribute to the extract's spectral profile.

3.2. FT-IR analysis

The introduction of PU and VTE into the Cs was confirmed by FT-IR spectroscopy (Fig. 4). The pristine chitosan spectrum exhibited characteristic absorption bands at 3338 cm^{-1} (O–H and N–H stretching), 2936 cm^{-1} (C–H stretching), 1638 cm^{-1} (amide I, $C = O$ stretching of residual N-acetyl groups), 1379 cm^{-1} (C–N stretching and –CH bending), 1319 cm^{-1} (C–O stretching), and 1257 cm^{-1} (C–O–C stretching) (Kalaycıoğlu et al., 2017). After grafting with PU, the band at 3338 cm^{-1} became

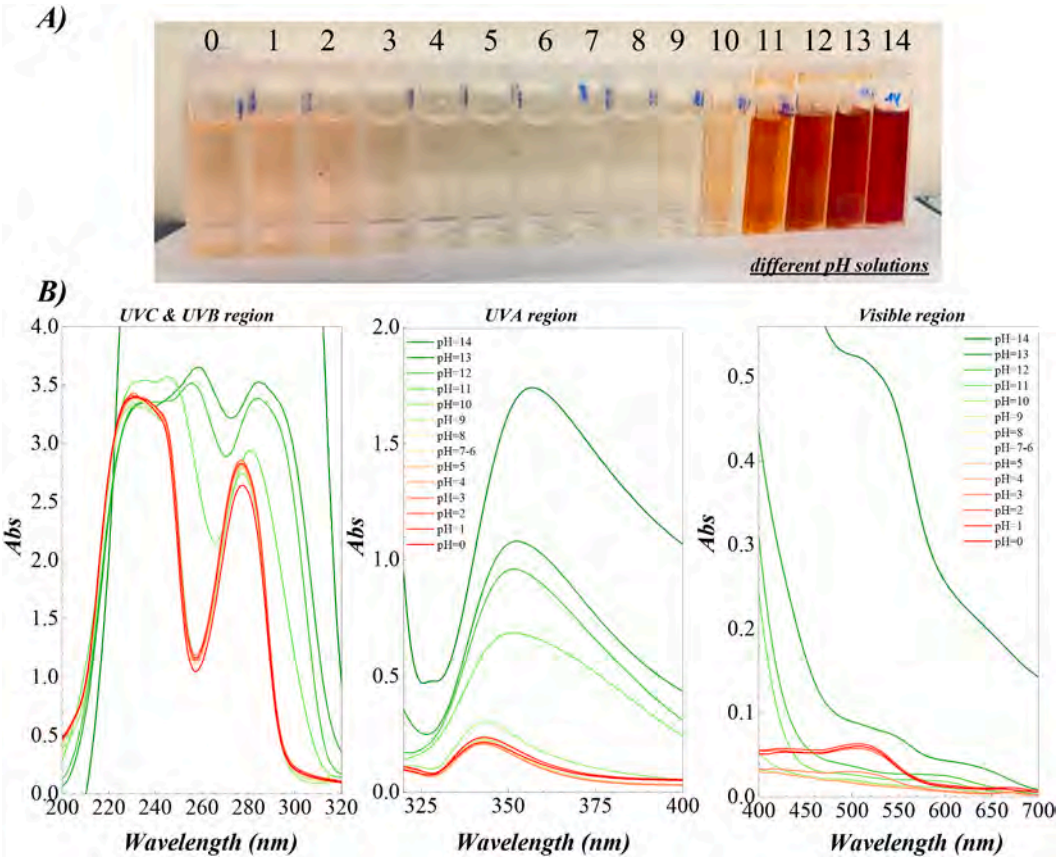

Fig. 2. Visual pH-sensitivity (A) and UV–Vis spectra (B) of 0.2 mg/mL of VTE solution in different pH solution.

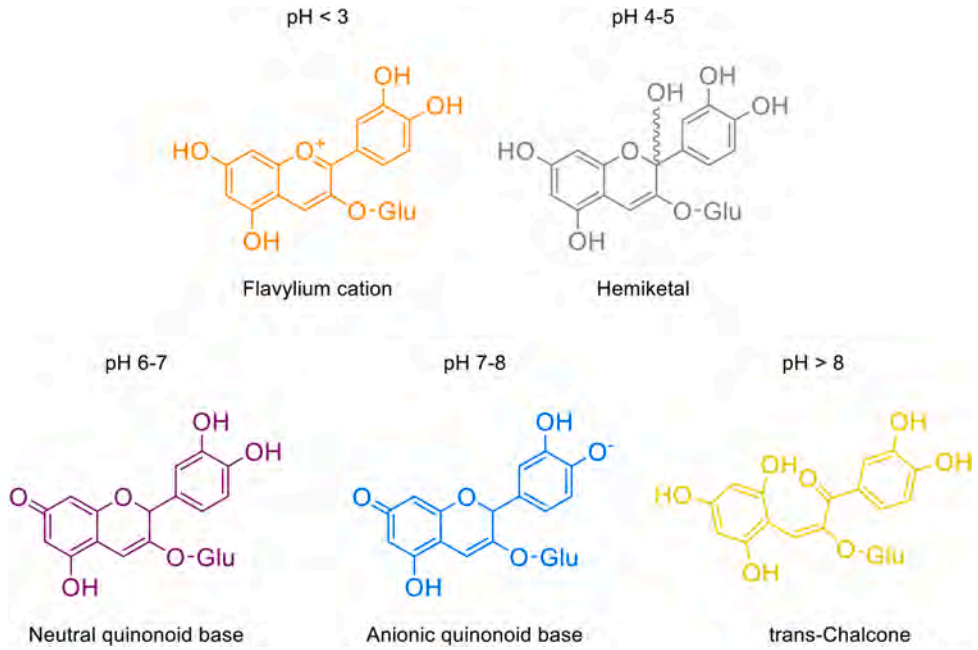

Fig. 3. Structural transformations of cyanidin-3-O-glycoside as a function of pH. Species are given with their expected colors (built based on the work of Houghton et al. (2021) and Pina et al. (2021)).

broader, while the intensity of the N–H bending band at 1557 cm^{-1} increased, both of which indicate the formation of hydrogen bonding between PU moieties and the chitosan backbone. Upon the incorporation of VTE, further modifications were observed with increasing extract concentration. The broad band at 3338 cm^{-1} became more intense and shifted slightly, reflecting additional hydrogen bonding interactions between hydroxyl groups of polyphenols and the amino/hydroxyl groups of the Cs–PU matrix (Qin et al., 2024). Additionally, a sharp band

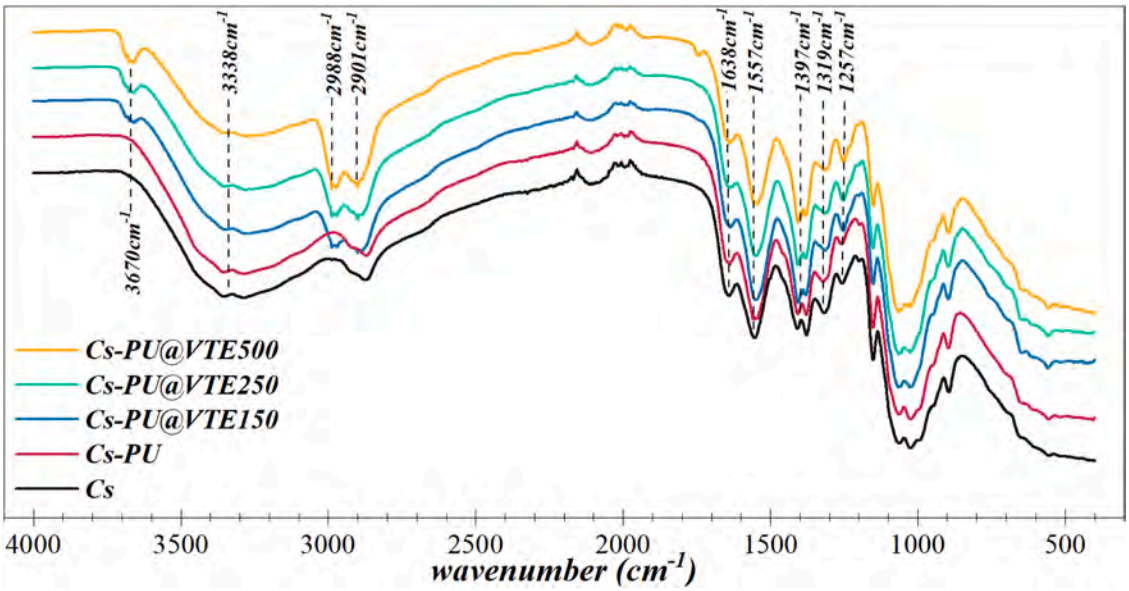

Fig. 4. FT-IR Spectra of Cs, Cs-PU, and Cs-PU@VTE films.

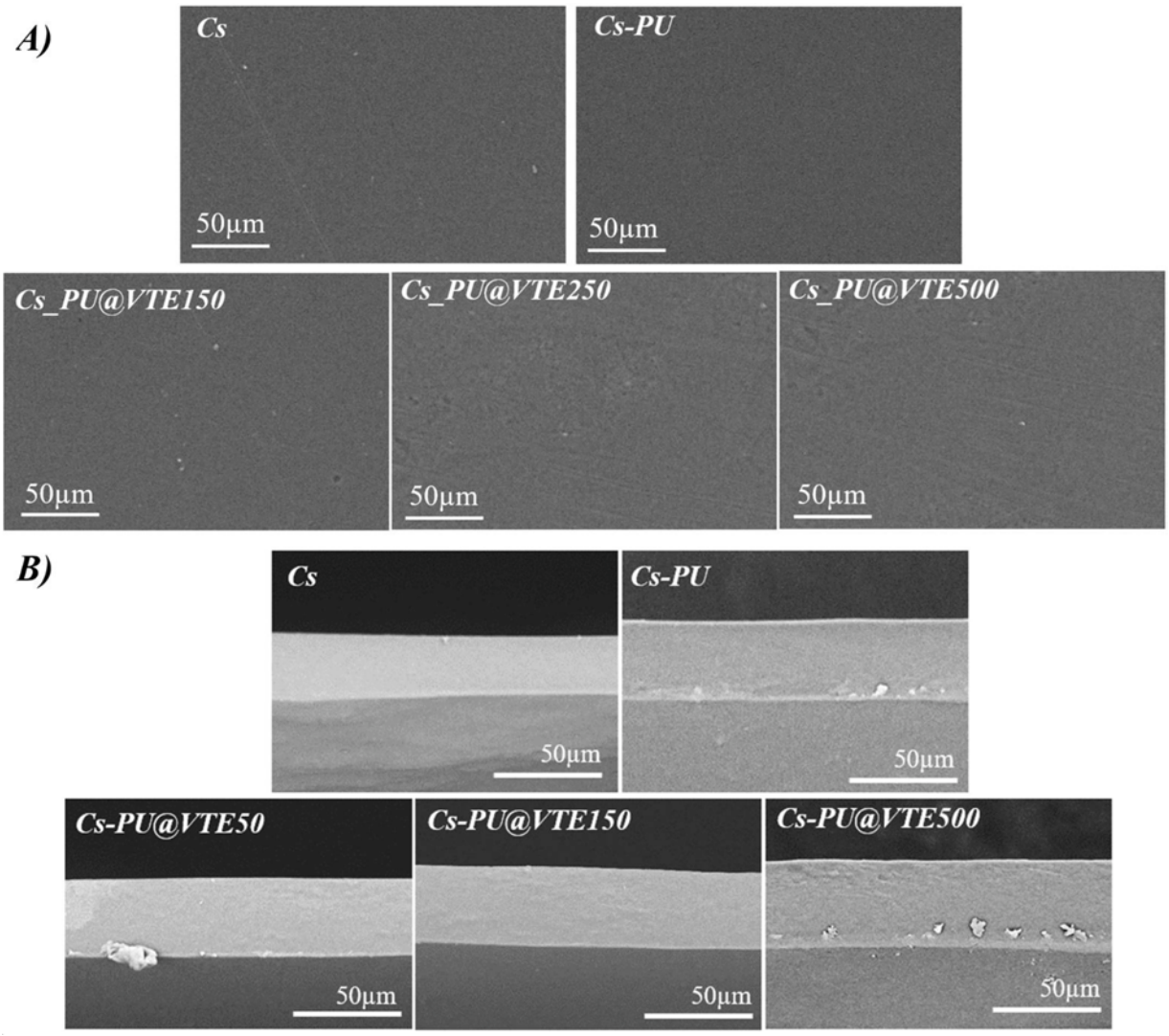

Fig. 5. Surface (A) and cross-section (B) SEM micrographs of pristine Cs. Cs-PU and different Cs-PU@VTE films.

appearing near ~3700 cm^{-1} can be attributed to isolated, non-hydrogen-bonded phenolic –OH groups from the VTE extract, consistent with the presence of free anthocyanin-related functionalities. Moreover, the peak at 1638 cm^{-1} broadened due to overlapping contributions from amide I vibrations and the carbonyl groups of the phenolic acids present in the extract. The gradual increase in the intensity of the 1379, 1319, and 1257 cm^{-1} bands also suggests interactions between the functional groups of VTE and the polymeric network.

3.3. SEM analysis

The surface morphology of pristine and functionalized Cs was analyzed through SEM. The obtained micrographs revealed a gradual change in surface morphology with the incorporation of PU and VTE into the chitosan matrix. The pristine Cs and Cs-PU films showed relatively smooth and uniform surfaces (Fig. 5A). However, incorporating VTE into the Cs-PU led to a progressive increase in surface roughness, which became more pronounced at higher VTE concentrations (Cs-PU@VTE250 and Cs-PU@VTE500), consistent with observations reported by other researchers (Qin et al., 2024). This increase in roughness may result from the formation of dispersed micro-domains or aggregates. Although no distinct particles were clearly visible on the surface, cross-sectional images (Fig. 5B) revealed a more heterogeneous and compact morphology for the Cs-PU and Cs-PU@VTE films compared to the pristine film, which exhibited a smooth cross section. These morphological changes likely reflect structural rearrangements within the polymer network. We speculate that π–π stacking interactions between the aromatic rings of the phenolic compounds in VTE and the phenyl groups grafted onto PU could promote such aggregation and enhance matrix cohesion. This interpretation is supported by the observed improvements in thermal and mechanical properties, suggesting that these micro-domains contribute to matrix reinforcement by restricting polymer chain mobility and enhancing stress distribution. (Chaudhary et al., 2021; Roy & Rhim, 2020)

3.4. Physical appearance and color parameters

The visual appearance of the films changed notably after the incorporation of phenylurea (PU) and increasing concentrations of VTE (Fig. 6). The pristine chitosan (Cs) film was smooth, colorless, and highly transparent. The introduction of PU (Cs–PU) did not markedly alter these features, as the film remained uniform and transparent. In contrast, the addition of VTE progressively modified the films: Cs-PU@VTE150 appeared light beige, Cs-PU@VTE250 became brownish with reduced clarity, and Cs-PU@VTE500 was darker and less transparent (Table 1). These changes are attributed to natural pigments in VTE, similar to effects reported with anthocyanin-enriched chitosan films (Qin et al., 2024). These observations are supported by color measurements (Table 1). The pure Cs film has a high lightness value (L) of 94.2 and very low red-green ('a' = 0.8) and yellow-blue ('b' = 2.1) values, confirming it is colorless and transparent. The Cs–PU film shows only a slight decrease in lightness (L = 92.5) and small increases in 'a' (1.2) and 'b' (2.8), which matches its clear, uniform appearance. When VTE is added to the films, lightness decreases as the amount of VTE increases. For Cs-PU@VTE150, the lightness is 86.3, while for sample Cs-PU@VTE250, it is 80.1, and for Cs-PU@VTE500, it is 72.7. This confirms that the films get darker with more extract content. At the same time, the 'a' value (red tint) increases from 2.6 for Cs-PU@VTE150 to 5.1 for sample Cs-PU@VTE500, while the 'b' value (yellow tint) rises strongly from 5.5 to 11.3. These variations account for the beige to brown appearance of the films, indicating that VTE incorporation introduces yellowish-brown pigmentation into the chitosan. Overall, the observed changes in color parameters demonstrate how increasing VTE content affects both the color and transparency of the films.

3.5. Moisture content, WVP and WCA

The influence of PU grafting and VTE incorporation on the moisture content, WVP and WCA of the chitosan films was also evaluated (Table 1), following the procedure described previously. Pristine chitosan exhibited the highest moisture content (23 %) because of the abundance of free hydroxyl and amino groups that strongly interact with water. After the introduction of PU, the value decreased to 21 %, and further decreased upon the addition of VTE, suggesting that the phenylurea groups and polyphenolic compounds limit the number of accessible polar sites for water binding (Souza et al., 2017). A similar trend was observed in WVP values. The pristine Cs film exhibited the highest permeability (3.5 10^{-11} $g.m^{-1}.s^{-1}.Pa^{-1}$), whereas the incorporation of PU and VTE led to a reduction in water vapor permeability. This reduction is attributed not only to increased hydrophobicity but also to the denser crosslinked network formed through hydrogen bonding. Such interactions create more tortuous diffusion pathways, thereby restricting water vapor transmission across the films (Sahraee et al., 2017; Yong et al., 2019). In our study, the Cs–PU and Cs-PU@VTE films achieved a WVP of 2.6 - 2.4 × 10^{-11} $g{\cdot}m^{-1}{\cdot}s^{-1}{\cdot}Pa^{-1}$, corresponding to ~ 26–30 % decrease compared with the unmodified Cs film. For comparison, Hasan et al. (2025) reported a WVP reduction from 8.48 × 10^{-8} to 4.89 × 10^{-8} $g{\cdot}Pa^{-1}{\cdot}s^{-1}{\cdot}m^{-1}$, representing a ~40 % decrease, but with a significantly higher anthocyanin content of 15 % in their PSPS–chitosan nanoparticle films. This highlights the efficiency of our PU-grafted chitosan matrix, where a substantial WVP reduction was achieved using only ~2 wt % of PU and ~6 wt % of VTE, demonstrating the synergistic effect of PU grafting and the phenolic-rich extract in improving barrier properties while maintaining lower additive content.

The water contact angle (WCA) results highlight the balance between hydrophobicity introduced by PU and hydrophilicity from VTE. Unmodified chitosan exhibited a WCA of 81.8°, reflecting its hydrophilic surface due to abundant hydroxyl and amino groups. Grafting with PU caused a sharp increase in the angle to 101.2°, indicating that phenyl rings and urea moieties imparted a strong hydrophobic character since they are present in approx. 2 wt % (see Table S1). With the incorporation of VTE, the WCA progressively decreased with concentration (98.3° → 95.2° → 91.8°), as the polyphenolic hydroxyl and carbonyl groups increased surface polarity, counteracting PU-induced hydrophobicity, and partially restoring wettability.

Fig. 6. Physical appearance of Cs, Cs-PU and Cs-PU@VTE films.

Table 1
Color parameters, moisture content, WVP, and WCA of Cs, Cs-PU, and Cs-PU@VTE.

Samples	*Cs*	*Cs-PU*	*Cs-PU@VTE150*	*Cs-PU@VTE250*	*Cs-PU@VTE500*
L	94 ± 5	92 ± 5	86 ± 4	80 ± 4	73 ± 4
a	0.80 ± 0.04	1.2 ± 0.1	2.6 ± 0.1	3.4 ± 0.2	5.1 ± 0.3
b	2.1 ± 0.1	2.8 ± 0.1	5.5 ± 0.3	8.9 ± 0.4	11 ± 1
ΔE	0.9 ± 0.1	1.9 ± 0.1	8.3 ± 0.2	16 ± 1	23 ± 1
WI	88 ± 1	84 ± 1	70 ± 1	53 ± 1	39 ± 1
YI	3.2 ± 0.1	4.3 ± 0.3	9.1 ± 0.2	16 ± 1	22 ± 1
Moisture content (%)	23 ± 2	21 ± 1	18 ± 1	19 ± 1	19 ± 1
WVP ($x10^{-11}$ $g.m^{-1}.s^{-1}.Pa^{-1}$)	03.5 ± 0.1	02.6 ± 0.1	02.5 ± 0.1	2.5 ± 0.1	02.4 ± 0.1
WCA (°)	81.8 ± 1.3	101.2 ± 1.7	98.3 ± 0.3	95.2 ± 0.4	91.8 ± 0.4
	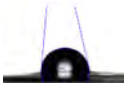				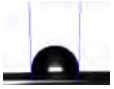

Data are expressed as mean ± SD. Measurements were performed in triplicate for all the measurements.

3.6. Thermal stability analysis

The thermal stability of the films was evaluated using thermogravimetric analysis (TGA) and derivative thermogravimetry (DTG). Chitosan films typically exhibit three characteristic weight-loss stages (Fig. 7). The first stage, occurring between 100 °C and 120 °C, corresponds to the loss of physically adsorbed water (~12 %). The second major weight loss, observed around 350–400 °C (~56 %), is attributed to the thermal degradation of the chitosan backbone. The final stage, near 600 °C (~32 %), relates to the decomposition of carbonaceous residues and the oxidative degradation of char in air (Bi et al., 2019). After functionalization with PU, a slight increase in thermal stability is observed (Fig. 7A and B). Upon the incorporation of VTE at increasing concentrations, a progressive shift in the main thermal degradation stage towards higher temperatures was observed compared to pure Cs and Cs–PU films. The DTG peaks became broader and less intense, indicating a more gradual degradation process. These results suggest that the phenolic compounds present in VTE enhance thermal resistance, likely through increased hydrogen bonding and the formation of a more compact, thermally stable matrix (Kaya et al., 2018; Qin et al., 2024). The Cs–PU@VTE500 sample exhibited the greatest thermal stability, with lower rate of weight loss. Overall, the combined effect of PU grafting and VTE incorporation improves the structural cohesion and heat resistance of the films, making them more suitable for applications requiring enhanced thermal durability.

3.7. Mechanical properties

The mechanical properties of the chitosan-based films were evaluated to understand the effects of phenylurea (PU) grafting and the incorporation of VTE at various concentrations. The unmodified chitosan film exhibited limited mechanical performance, with low tensile strength, poor elongation at break, and a relatively low Young's modulus, reflecting its inherent brittleness (Fig. 8). Grafting with PU (Cs-PU) led to a noticeable improvement in all these mechanical properties. This enhancement is attributed to additional intermolecular interactions, including hydrogen bonding and π–π stacking between the phenyl groups of PU, which serve to reinforce the chitosan matrix and increases it Young's modulus by 50 %. Further incorporation of VTE extract at increasing concentrations resulted in a progressive and consistent enhancement in tensile strength, elongation at break, and Young's modulus. These improvements suggest that the phenolic and

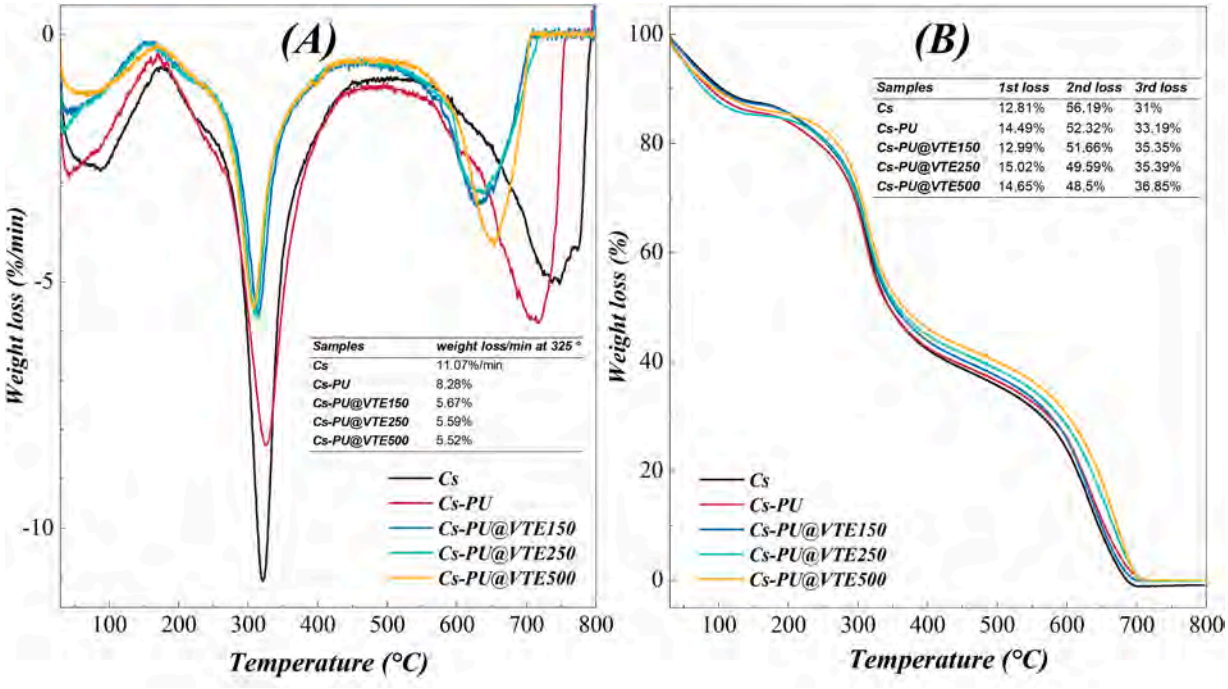

Fig. 7. (A) DTG and (B) TGA curves of pristine Cs, Cs-PU and Cs-PU@VTE films.

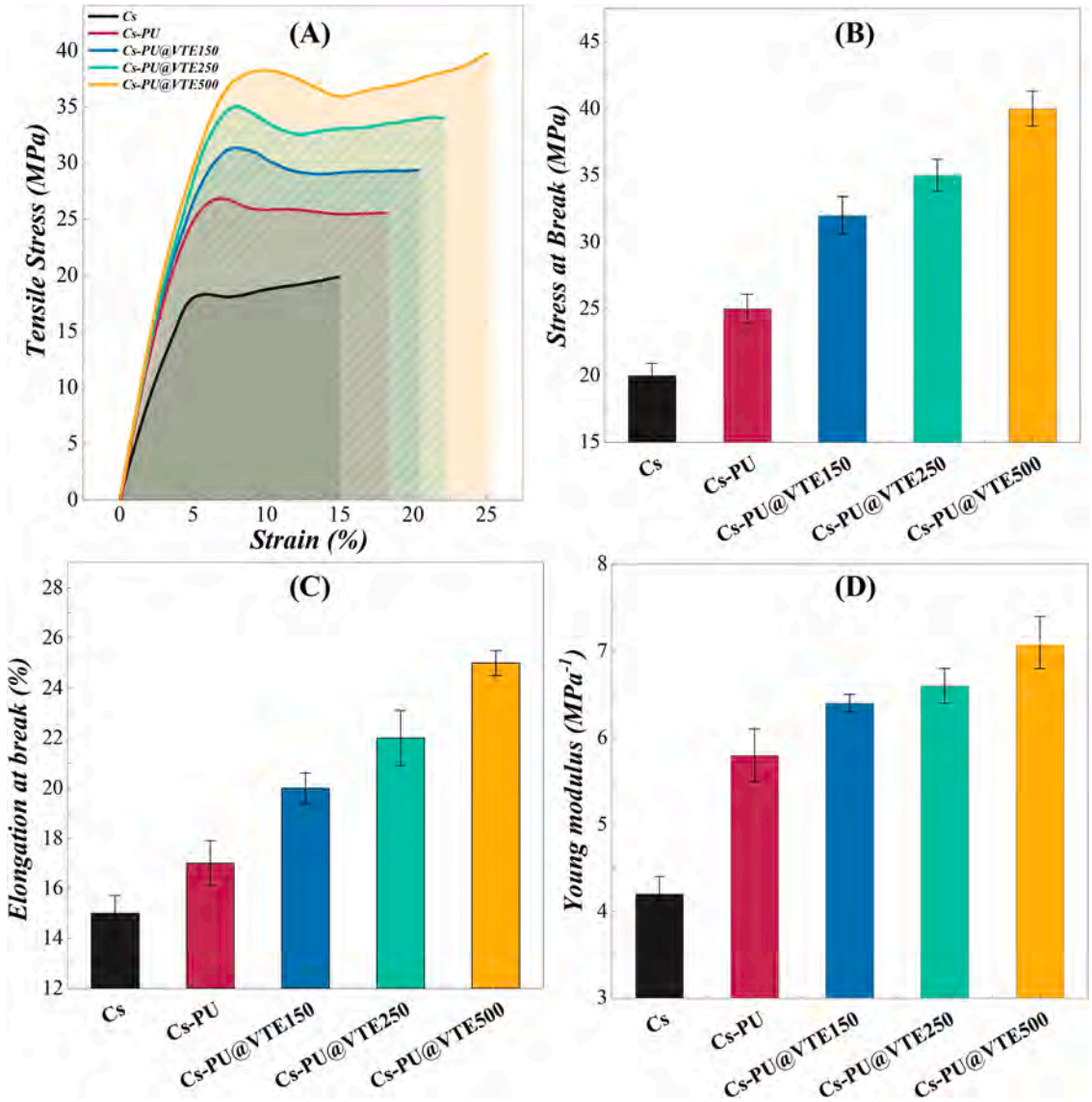

Fig. 8. Mechanical characterization of Cs, Cs-PU, and Cs-PU@VTE films: (A) representative stress-strain curves highlighting the toughness area, (B) tensile strength at break, (C) elongation at break, and (D) Young's modulus values.

the flavonoid compounds present in the extract act as physical cross-linkers or plasticizers within the polymer network (Gómez-Guillén et al., 2007; Siripatrawan & Harte, 2010). In our study, the Cs–PU@VTE500 film exhibited a 100 % increase in tensile strength and a 75 % increase in Young's modulus, representing a marked improvement compared with previous reports. For comparison, Hasan et al. (2025) reported that incorporating purple sweet potato anthocyanin extract into chitosan/purple sweet potato starch bio-nanocomposite films increased tensile strength by ~72 %, while Alnadari et al. (2023) observed that carboxymethyl chitosan/gum Arabic films containing ~1.5 % anthocyanins showed more modest improvements, with a ~13 % increase in tensile strength and a ~30 % increase in elongation at break. In our system, the Cs–PU@VTE250 film, which has a comparable extract-to-chitosan ratio of ~1.67 %, displayed a 75 % increase in tensile strength, a 62.5 % increase in Young's modulus, and a 46.7 % increase in elongation at break. These findings underscore the strong synergistic effect of PU grafting and VTE incorporation, which reinforces the chitosan matrix and acts as a plasticizer, achieving superior mechanical performance even at similar extract loadings. As the VTE content increased, the matrix became more compact and better organized, facilitating more efficient stress transfer and enhanced mechanical resistance. Notably, the Cs–PU@VTE500 film showed the highest mechanical performance, indicating a synergistic effect between PU grafting and high VTE loading. Overall, these results confirm that both PU modification and the phenolic-rich extract significantly contribute to improving the structural integrity, flexibility, and strength of chitosan films.

3.8. Light barrier properties

The UV transmission spectra of Cs, Cs–PU, and Cs–PU films incorporated with increasing amounts of VTE, reveal important insights into their potential as UV-blocking materials (Fig. 9). Pristine chitosan films exhibited high transmittance (> 90 %) in the visible region (> 400 nm), with partial blocking only in the deep UV range (< 300 nm), which is due to the transparency and the absence of UV absorber chromophore in chitosan structure (Yong et al., 2019). Upon grafting with phenylurea groups, a slight improvement in UV-blocking was observed (Fig. 9) due to increased aromatic content that can absorb in the UVC region (Rajesh Shukla et al., 2012). More significantly, the addition of VTE extract caused a marked decrease in transmittance in the UV range (250–400 nm) (Fig. 9A), especially as the VTE concentration increased. The

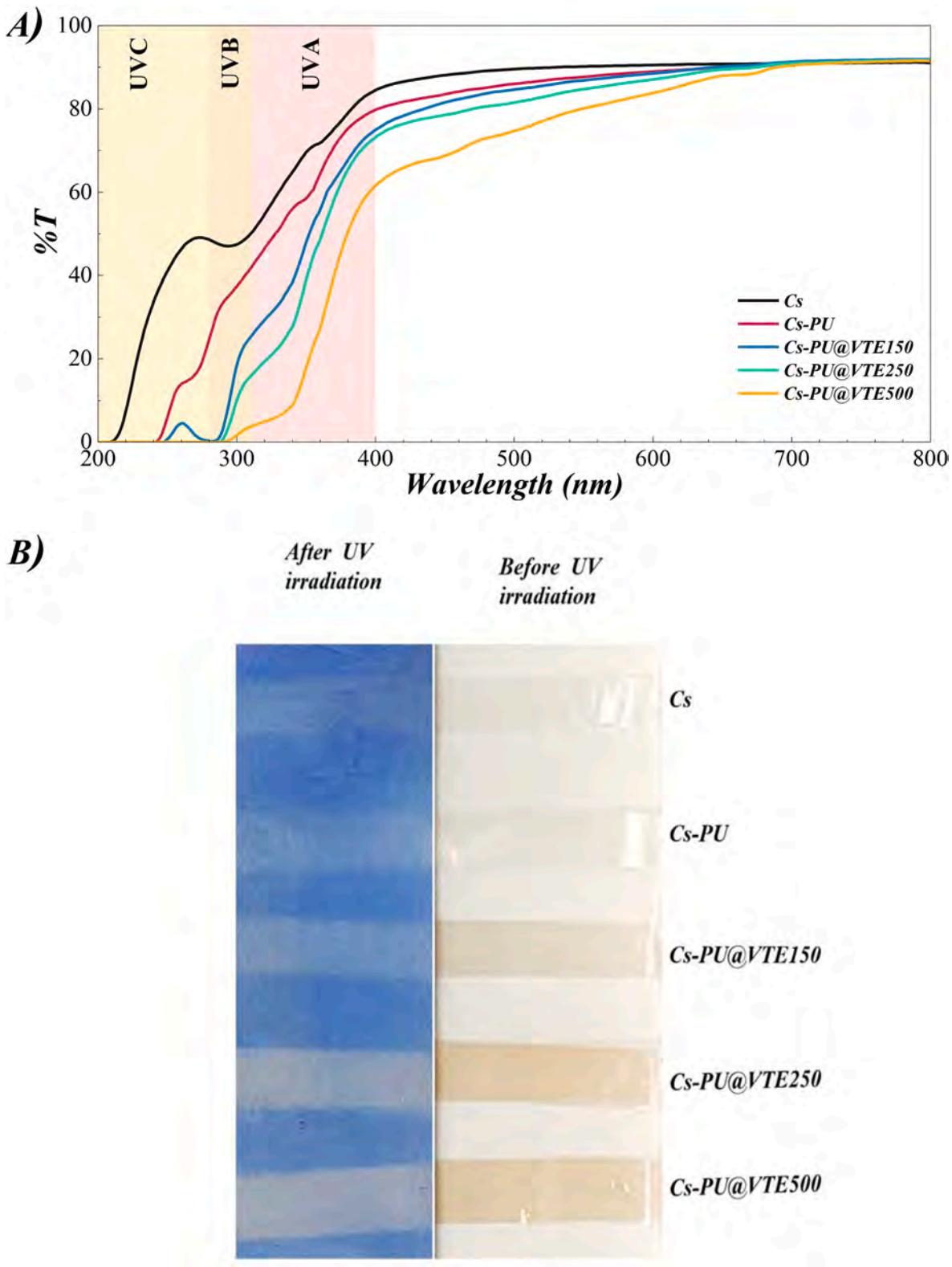

Fig. 9. UV–Vis spectrum of (A) Cs, Cs-PU and Cs-PU@VTE, and (B) dye-activation protection test (bottom).

Cs-PU@VTE500 exhibited the strongest UV-shielding effect, with zero transmittance between 200 and 300 nm and <60 % transmittance between 350 and 400 nm, while maintaining substantial transparency in the visible range. This behavior can be attributed to the rich content of phenolic compounds, particularly anthocyanins and flavonoids, in the VTE extract (Wang et al., 2019; Yong et al., 2019). For comparison, Xu et al. (2025) reported that chitosan-based films containing black rice anthocyanin achieved zero transmittance in the UV region (<400 nm); however, this was accompanied by low transmittance in the visible region, resulting in darker, less transparent films. In contrast, our Cs–PU@VTE films provide strong UV protection while retaining higher visible-light transparency, demonstrating a favorable balance between

UV-shielding and film clarity. This highlights the advantage of VTE incorporation in PU-grafted chitosan matrices, allowing effective UV-blocking without compromising optical quality. Moreover, this potential was further demonstrated by the dye-activation protection test (Fig. 9B). In this test, the films were used to prevent a spiropyran-based dye inserted into a paper sheet from changing color (i.e. turning blue) and conformation. The films containing the VTE resulted to effectively block UV-induced dye activation, with the Cs-PU@VTE500 providing the highest protection. This confirmed the protective ability of VTE, as expected based on their phenolic content.

3.9. pH sensitivity

To evaluate the pH sensitivity of the films, samples were submerged in 8 different pH solutions for 2 min. The samples were then recovered and dried, and the color change was recorded. Below, we only report the results for the samples containing VTE, since pristine Cs and functionalized Cs-PU did not exhibit any color change across the entire pH range (see **Fig. S5**). Increased VTE loadings produced an evident color response across the tested pH range (Fig. 10B). Under neutral to mildly alkaline conditions (pH 6–8), the color of the films shifted from beige to a yellowish-green hue. This shift was most pronounced in the high-VTE formulation (Cs-PU@VTE500) and resembled anthocyanin behavior. In acidic media (pH 0–4), the films largely preserved their original color, although they appeared lighter and display a faint red-pink hue at very low pH (0–2) (Fig. 10B). The most striking changes occurred under strongly alkaline conditions (pH $\geq$ 9), where the films turned a deep reddish-brown color. This reflected the deprotonation and structural transformation of the anthocyanin dyes (Qin et al., 2024). Quantitative analysis of the *Lab** color parameters clearly supported the visual

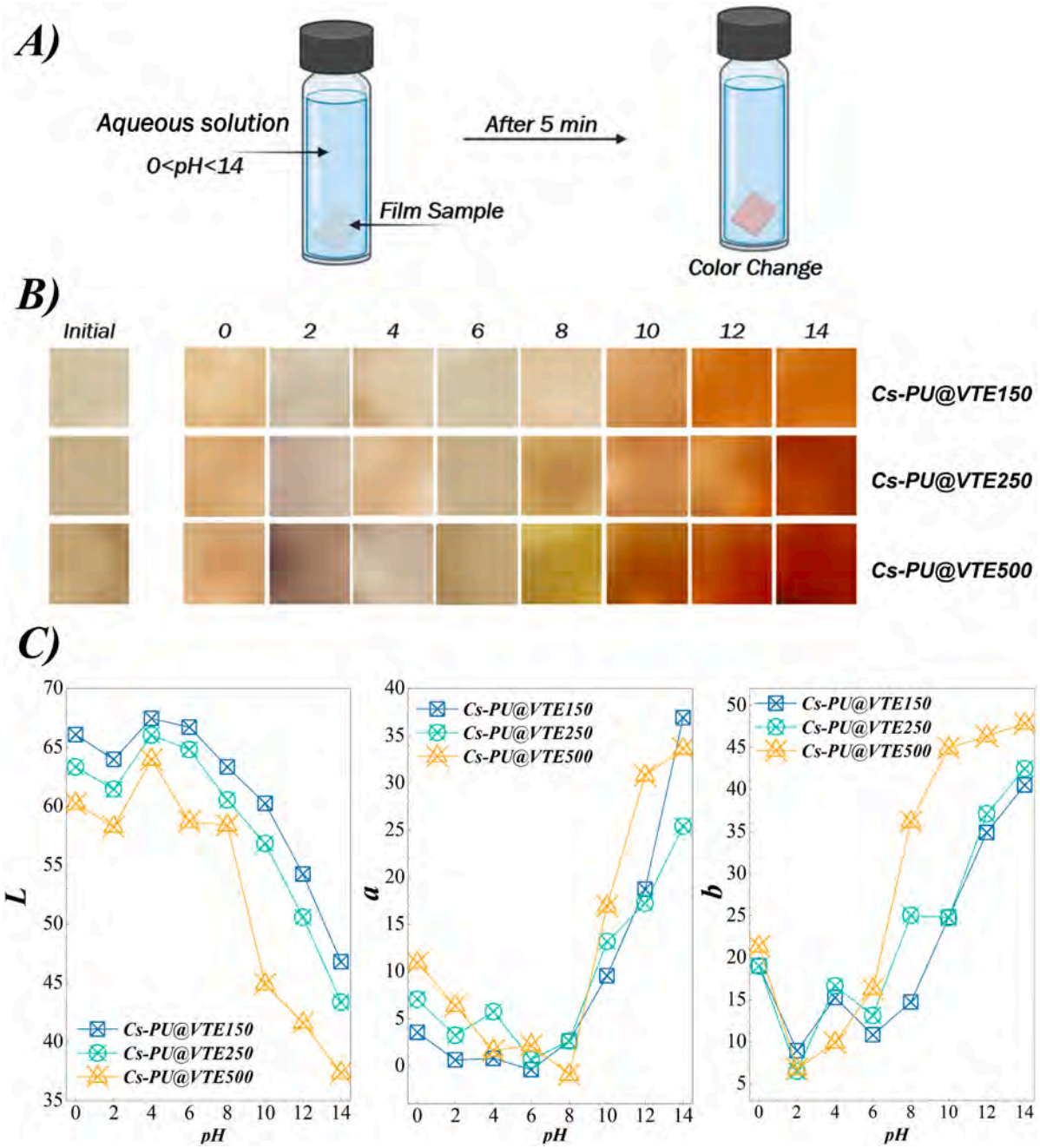

Fig. 10. Representation of pH-sensitivity test (A), color variation of Cs-PU@VTE films at different pH (B), and effect of pH on Cs-PU@VTE color parameters (C).

changes observed in the pH sensitivity test of the chitosan films (Fig. 10C). As the pH shifted from acidic or neutral to strongly alkaline, the '*L*' values decreased markedly, confirming that the films became progressively darker. At the same time, the '*a*' parameter, reflecting the red–green axis, showed a sharp increase to highly positive values under alkaline conditions, which explains the strong reddish tones visible at higher pH values. Similarly, the '*b*' parameter, representing the yellow–blue axis, increased significantly with alkalinity, reaching its highest values at pH 12–14. This directly corresponds to the intense yellow-brown coloration observed in the films. Increasing the anthocyanin extract concentration (Cs-PU@VTE500 compared to Cs-PU@VTE150) enhanced both color intensity and pH sensitivity confirming the of the extract's effectiveness as a pH indicator.

3.10. Ammonia sensitivity

pH-responsive films can provide a simple, non-invasive, and easily interpretable visual indicator for food freshness. They are particularly relevant for protein-rich foods such as meat, poultry, and seafood, as these release ammonia and amines during spoilage, which leads to an increase in local pH (Gasti et al., 2021). Therefore, testing the films' response to ammonia provides a practical way of evaluating their ability to detect the alkaline vapors associated with food deterioration (Chen et al., 2020). To this end, we exposed the synthesized films containing the VTE that exhibited in the pH sensitivity test visible color change to ammonia vapors, and we recorded the color change at 10-minutes intervals up to 30 min. Upon exposure to ammonia gas, the films gradually and markedly changed color, shifting towards reddish-brown and orange hues (Fig. 11). This response was quantitatively supported by decreasing '*L*' values, indicating reduced lightness, and increasing '*a*' and '*b*' parameters, reflecting growth in red and yellow tones, respectively. This was attributed to the chromatic transformation of the incorporated anthocyanin extract, which undergoes structural changes when interacting with volatile alkaline compounds (Jiang et al., 2023). The magnitude and speed of the color change were particularly pronounced in Cs-PU@500VTE, which contains the higher amount of extract, and were proportional to the duration of contact with ammonia vapors.

3.11. Antioxidant activity

One of the most widely used methods for evaluating the antioxidant properties of substances is the DPPH radical scavenging assay. The antioxidant acts by neutralizing DPPH free radicals through electron or

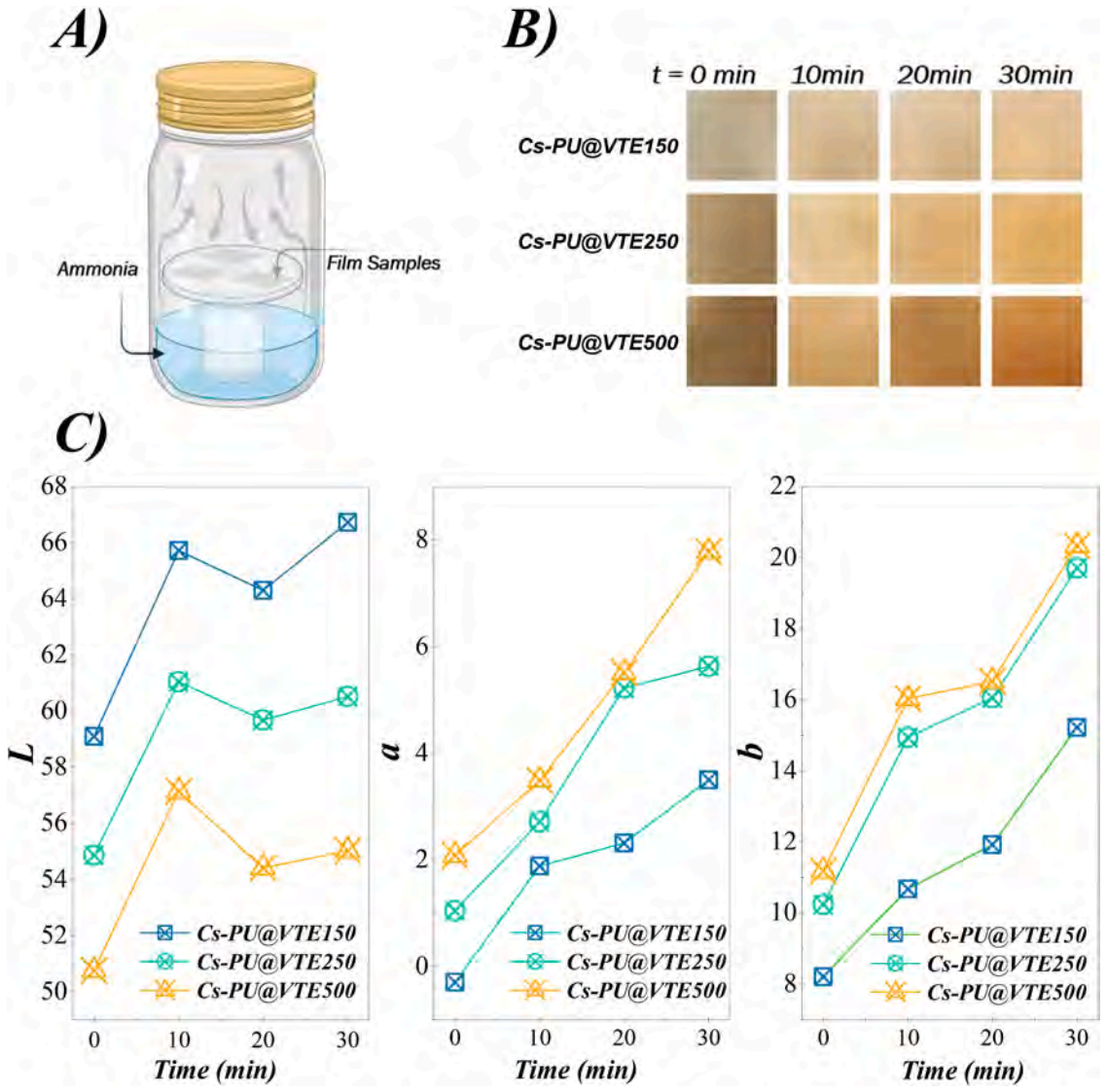

Fig. 11. Representation of Ammonia-sensitivity test (A), color variation of Cs-PU@VTE films over exposure time (B), variation of Cs-PU@VTE color parameters over exposure to ammonia (C).

hydrogen atom donation, resulting in a measurable decrease in absorbance that reflects their scavenging capacity (Saravanakumar et al., 2020). The DPPH radical scavenging assay highlighted the marked improvement in antioxidant performance of chitosan films following the incorporation of the anthocyanin-rich VTE extract (Fig. 12). Both pristine Cs and Cs-PU demonstrated minimal and nearly identical activity, with an inhibition of ~5 % (orange and red curves in Fig. 12). On the contrary, Cs-PU@VTE films demonstrate a significant and concentration-dependent increase in radical scavenging capacity. Specifically, Cs-PU@VTE500 achieves the highest inhibition, reaching almost 38 % after three hours, followed by Cs-PU@VTE250 at around 26 % and Cs-PU@VTE150 at around 21 %. This enhancement is directly attributable to the incorporation of anthocyanins, which are known for their powerful antioxidant properties and ability to neutralize free radicals via hydrogen atom transfer (HAT) and single electron transfer (SET). (Qin et al., 2024; Wang et al., 2019; Yong et al., 2019). The gradual, time-dependent increase in scavenging activity further supports that these groups remain active within the film matrix, effectively interacting with the DPPH radicals over time.

3.12. Food-freshness monitoring test

During the storage of Atlantic cod (*Gadus morhua*), the release of volatile amines is a well-established indicator of spoilage and freshness loss, as these compounds are responsible for the characteristic fishy odor associated with protein degradation. In this study, Cs-PU@VTE films were used as intelligent colorimetric indicator labels in the headspace of sealed containers containing fish samples. As shown in Fig. 13A, all films exhibited a visible color change after 24 h at 25 °C, indicating the rapid onset of spoilage. Among them, Cs-PU@VTE500 showed the highest sensitivity, shifting from green-yellow to light pink-orange within 24 h and to dark orange after 48 h. These visual changes were quantitatively confirmed by CIELAB analysis (Fig. 13B). While lightness (L*) and yellowness (b*) increased for all samples, the most significant variation was observed in the a* parameter. For Cs-PU@VTE500, a* shifted from −4 (green) to +4 (red), crossing the neutral point and producing the characteristic orange-pink hue, while b* reached 35, the highest among all films. This behavior reflects a strong interaction between volatile amines and the responsive components of the film matrix. Comparable responses have been reported for anthocyanin-based chitosan indicators. Pang et al. (2023) observed complete color changes within 48 h in chitosan-based films containing purple sweet potato anthocyanins, consistent with TVB-N evolution, while Li et al. (2021) reported progressive color transitions in purple tomato anthocyanin-loaded chitosan films over 48 h at ~23 °C. Compared to these systems, Cs-PU@VTE films, particularly Cs-PU@VTE500, exhibited a faster and more intense chromogenic response within the first 24 h, highlighting their potential for early spoilage detection.

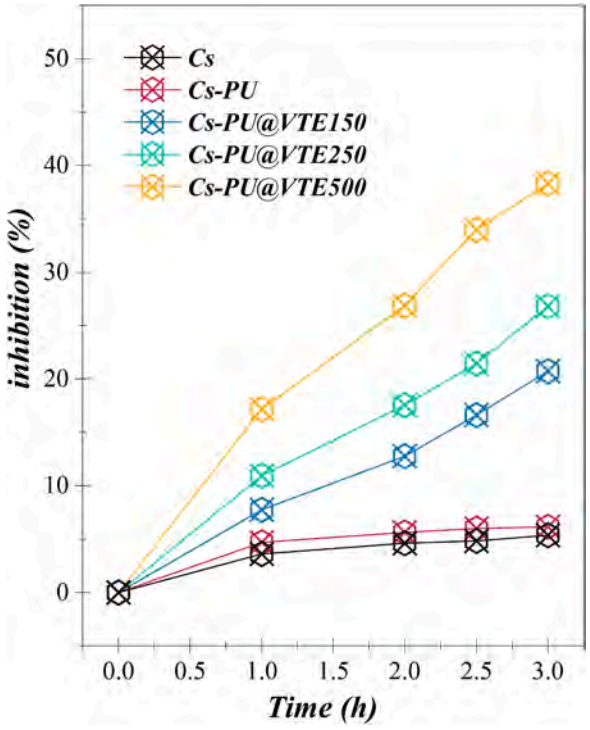

Fig. 12. DPPH scavenging activity of pristine Cs and Cs-modified films.

3.13. Film integrity and stability analysis

The structural performance of the bio-based films strongly depended on environmental conditions. It is known that when fully submerged in water, chitosan films showed high sensitivity and disintegration, mainly due to the low molecular weight of the chitosan backbone, which limits chain entanglement and resistance to hydration (Kubota & Eguchi, 1997). For this reason, we decided to apply the chitosan films as labels in cod fish packaging, and we monitored the film integrity for 48 h. As shown in Fig. 13, the films maintained structural integrity throughout the monitoring period, demonstrating adequate stability under humid conditions. Moreover, the films exhibited excellent colorimetric stability. As shown in Fig. S7, no significant visual color changes were observed after one month of storage at room temperature, indicating effective stabilization of V. tinus anthocyanins within the grafted chitosan network. This finding is consistent with previous reports showing that polymer matrices can protect anthocyanins from oxidation and environmental degradation, ensuring reliable long-term performance of colorimetric indicators (Kossyvaki et al., 2022).

3.14. Safety and regulatory considerations

From a food-contact perspective, the incorporation of botanical extracts into packaging materials requires careful evaluation of both regulatory compliance and migration behavior. In the European Union, overall migration from food-contact materials is limited to 60 mg·kg^{-1} of food or food simulant, corresponding to 10 mg·dm^{-2}, with specific migration limits established for individual substances ((Grob et al., 2007); EU Regulation No 10/2011). Based on the casting area of the films (0.709 dm^2), the loading of *Viburnum tinus* extract (VTE) corresponds to approximately 2.8 – 9.4 mg·dm^{-2}, depending on the extract concentration. These values remain below the regulatory threshold, even under the conservative assumption of complete migration. In principle, both overall and specific migration tests should be performed using appropriate food simulants in accordance with EU Regulation No 10/2011. However, in the present study, such tests could not be reliably conducted because the developed films are based on a chitosan matrix, which is soluble in several of the prescribed simulants, thereby preventing accurate migration measurements. This limitation should be acknowledged, and comprehensive migration and toxicological assessments will be required in future studies to fully evaluate regulatory compliance. Ethanol was selected as the extraction solvent for the VT due to its food-grade status, and its residual levels were assessed by HS GC–MS analysis. Very low concentrations of residual ethanol were detected ($< 2 \times 10^{-3}$ μg·m^{-2}), confirming the suitability of the preparation process from a safety perspective. Overall, although further investigations using alternative functionalization strategies and more stable chitosan-based systems are necessary to ensure full compliance with food-contact regulations, the present work provides a safe proof-of-concept for the development of V. tinus-based smart packaging materials.

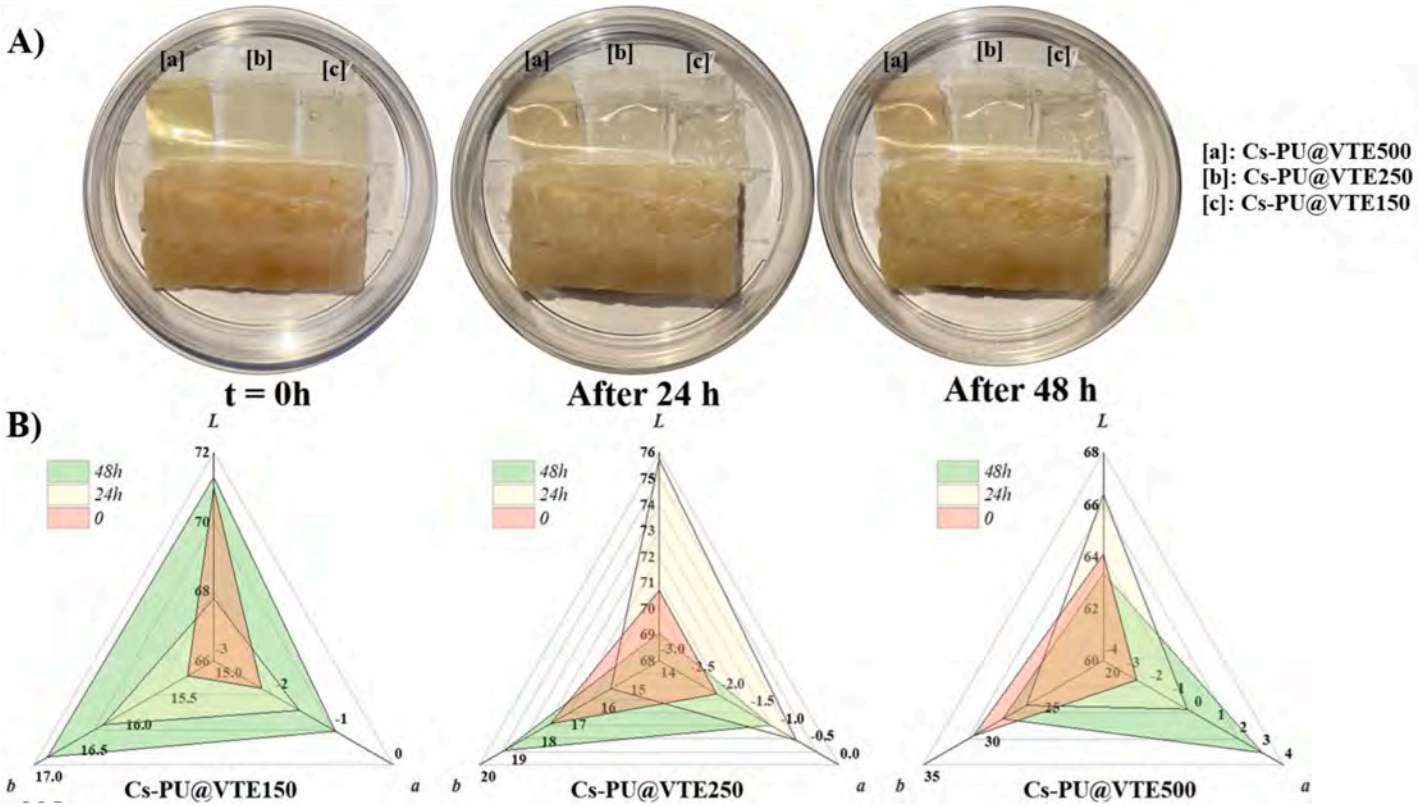

Fig. 13. Images of Cs-PU@VTE label films monitoring Atlantic Cod freshness (A), and color parameter of the film labels during storage (B).

4. Conclusion

This study demonstrates that combining phenylurea-functionalized chitosan with *Viburnum tinus* fruit extract provides an effective strategy for developing multifunctional bio-based films. The covalent grafting of phenylurea groups onto chitosan played a fundamental role in enhancing film performance, yielding improved mechanical strength (~25 % increase in tensile strength), increased hydrophobicity (WCA 81.8° → 101.2°), and a reduced water vapor permeability (WVP 3.5 → 2.6 × 10^{-11} g·m^{-1}·s^{-1}·Pa^{-1}). The incorporation of VTE preserved these improvements while introducing pH-sensitive color changes and enhanced UV protection; notably, VTE slightly decreased surface hydrophobicity compared to Cs–PU (WCA 98.3°–91.8° depending on loading), although all VTE-containing films remained more hydrophobic than pristine chitosan. As a proof-of-concept application, Cs–PU@VTE films showed strong potential as intelligent packaging labels, exhibiting rapid and sensitive colorimetric responses to volatile amines released during Atlantic cod spoilage, with clear visual changes within 24 h at room temperature (Cs–PU@VTE500 showing the highest sensitivity). From a safety perspective, the estimated VTE loading remained below the EU overall migration limit under the conservative assumption of complete migration; however, comprehensive migration and toxicological assessments, as well as formal regulatory evaluation of *V. tinus* for food-contact uses, should be addressed in future studies.

CRediT authorship contribution statement

Mouad El Mouzahim: Writing – review & editing, Writing – original draft, Methodology, Investigation, Formal analysis, Data curation, Conceptualization. **Alessandro Pedrini:** Writing – review & editing, Supervision, Methodology, Data curation. **Enrico Dalcanale:** Writing – review & editing, Validation, Methodology, Data curation, Conceptualization. **N. Riboni:** Validation, Formal analysis. **F. Bianchi:** Validation, Formal analysis, Data curation. **A. Jorge Parola:** Writing – review & editing, Supervision, Data curation, Conceptualization. **Roberta Pinalli:** Writing – review & editing, Writing – original draft, Supervision, Resources, Project administration, Funding acquisition, Conceptualization.

Declaration of competing interest

The authors declare that they have no known competing financial interests or personal relationships that could have appeared to influence the work reported in this paper.

Acknowledgments

The Authors acknowledge the project VIT, funded through the European Union Horizon 2020 Program (H2020-MSCA-RISE-2020, grant agreement no 101008237). This work also benefited from the equipment and support provided by the COMP-HUB and COMP-R Initiatives, funded under the 'Departments of Excellence' program of the Italian Ministry for University and Research (MIUR, 2018–2022; MUR, 2023–2027). The first author extends his thanks to the National Recovery and Resilience Plan (**PNRR**), Mission 4 Component 2 Investment 3.3 - Call for tender No 352 of 09/04/2022 of Italian Ministry of University and Research funded by the European Union – NextGenerationEU, and Intercos Group for the financial support. The authors further acknowledge the Centro Interfacoltà di Misure "G. Casnati" of the University of Parma for access to NMR facilities. The authors also thank **Professor Dr. Luísa Neves** of the NOVA School of Science and Technology, Lisbon, for kindly providing access to the scanning electron microscopy (SEM) facility, and **Professor Dr. Filomena Freitas**, of the same institution, for granting access to the texturometer, both of which were essential to the successful completion of this study.

Supplementary materials

Supplementary material associated with this article can be found, in the online version, at doi:10.1016/j.carpta.2026.101103.

Data availability

Data will be made available on request.

References

Alnadari, F., Al-Dalali, S., Pan, F., Abdin, M., Frimpong, E. B., Dai, Z., Al-Dherasi, A., & Zeng, X. (2023). Physicochemical characterization, molecular modeling, and applications of carboxymethyl chitosan-based multifunctional films combined with gum arabic and anthocyanins. *Food and Bioprocess Technology, 16*(12), 2984–3002. https://doi.org/10.1007/s11947-023-03122-0

Amaregouda, Y., Kamanna, K., & Gasti, T. (2022). Fabrication of intelligent/active films based on chitosan/polyvinyl alcohol matrices containing Jacaranda cuspidifolia anthocyanin for real-time monitoring of fish freshness. *International Journal of Biological Macromolecules, 218*, 799–815. https://doi.org/10.1016/j.ijbiomac.2022.07.174

Berger, J., Reist, M., Mayer, J. M., Felt, O., Peppas, N. A., & Gurny, R. (2004). Structure and interactions in covalently and ionically crosslinked chitosan hydrogels for biomedical applications. *European Journal of Pharmaceutics and Biopharmaceutics, 57*(1), 19–34. https://doi.org/10.1016/S0939-6411(03)00161-9

Bi, F., Zhang, X., Bai, R., Liu, Y., Liu, J., & Liu, J. (2019). Preparation and characterization of antioxidant and antimicrobial packaging films based on chitosan and proanthocyanidins. *International Journal of Biological Macromolecules, 134*, 11–19. https://doi.org/10.1016/j.ijbiomac.2019.05.042

Cazón, P., & Vázquez, M. (2020). Mechanical and barrier properties of chitosan combined with other components as food packaging film. *Environmental Chemistry Letters, 18*(2), 257–267. https://doi.org/10.1007/s10311-019-00936-3

Chaudhary, B. U., Lingayat, S., Banerjee, A. N., & Kale, R. D. (2021). Development of multifunctional food packaging films based on waste garlic peel extract and chitosan. *International Journal of Biological Macromolecules, 192*(October), 479–490. https://doi.org/10.1016/j.ijbiomac.2021.10.031

Chen, H. Z., Zhang, M., Bhandari, B., & Yang, C. H. (2020). Novel pH-sensitive films containing curcumin and anthocyanins to monitor fish freshness. *Food Hydrocolloids, 100*, Article 105438. https://doi.org/10.1016/j.foodhyd.2019.105438

Choo, K. W., Lin, M., & Mustapha, A. (2021). Chitosan/acetylated starch composite films incorporated with essential oils: Physiochemical and antimicrobial properties. *Food Bioscience, 43*, Article 101287. https://doi.org/10.1016/j.fbio.2021.101287

Cometa, M. F., Mazzanti, G., & Tomassini, L. (1998). Sedative and spasmolytic effects of *Viburnum tinus* L. and its major pure compounds. *Phytotherapy Research, 12*(SUPPL. 1), S89–S91. https://doi.org/10.1002/(SICI)1099-1573(1998)12:1+<S89::AID-PTR260>3.0.CO;2-T

Frank, K., Garcia, C. V., Shin, G. H., & Kim, J. T. (2018). Alginate biocomposite films incorporated with cinnamon essential oil nanoemulsions: Physical, mechanical, and antibacterial properties. *International Journal of Polymer Science, 2018*, Article 1519407. https://doi.org/10.1155/2018/1519407

Gasti, T., Dixit, S., D'souza, O. J., Hiremani, V. D., Vootla, S. K., Masti, S. P., Chougale, R. B., & Malabadi, R. B (2021). Smart biodegradable films based on chitosan/methylcellulose containing Phyllanthus reticulatus anthocyanin for monitoring the freshness of fish fillet. *International Journal of Biological Macromolecules, 187*, 451–461. https://doi.org/10.1016/j.ijbiomac.2021.07.128

Gómez-Guillén, M. C., Ihl, M., Bifani, V., Silva, A., & Montero, P. (2007). Edible films made from tuna-fish gelatin with antioxidant extracts of two different murta ecotypes leaves (Ugni molinae Turcz). *Food Hydrocolloids, 21*(7), 1133–1143. https://doi.org/10.1016/j.foodhyd.2006.08.006

Grob, K., Pfenninger, S., Pohl, W., Laso, M., Imhof, D., & Rieger, K. (2007). European legal limits for migration from food packaging materials: 1. Food should prevail over simulants; 2. More realistic conversion from concentrations to limits per surface area. PVC cling films in contact with cheese as an example. *Food Control, 18*(3), 201–210. https://doi.org/10.1016/j.foodcont.2005.09.015

Haghighi, H., Licciardello, F., Fava, P., Siesler, H. W., & Pulvirenti, A. (2020). Recent advances on chitosan-based films for sustainable food packaging applications. *Food Packaging and Shelf Life, 26*, Article 100551. https://doi.org/10.1016/j.fpsl.2020.100551

Hamann, D. R., Shukla, A., Platzman, P. M., & Isaacs, E. D. (2001). Hydrogen bonding in urea. *Physical Review B - Condensed Matter and Materials Physics, 64*(5), Article 52101. https://doi.org/10.1103/PhysRevB.64.052101

Han, J. W., Ruiz-Garcia, L., Qian, J. P., & Yang, X. T. (2018). Food packaging: A comprehensive review and future trends. *Comprehensive Reviews in Food Science and Food Safety, 17*(4), 860–877. https://doi.org/10.1111/1541-4337.12343

Hasan, M., Utami, A., Siregar, C., Hanum, L., Khaldun, I., & Nazar, M. (2025). Thermal, structural and mechanical characterization of bio-nanocomposite films from purple sweet potato starch/chitosan nanoparticles integrated with anthocyanin extract. *Results in Engineering, 25*, Article 104448. https://doi.org/10.1016/j.rineng.2025.104448

Hossain, F., Follett, P., Salmieri, S., Vu, K. D., Fraschini, C., & Lacroix, M. (2019). Antifungal activities of combined treatments of irradiation and essential oils (EOs) encapsulated chitosan nanocomposite films in in vitro and in situ conditions.

International Journal of Food Microbiology, 295, 33–40. https://doi.org/10.1016/j.ijfoodmicro.2019.02.009

Houghton, A., Appelhagen, I., & Martin, C. (2021). Natural blues: Structure meets function in anthocyanins. *Plants, 10*(4), 726. https://doi.org/10.3390/plants10040726

Jiang, C., Liu, T., Wang, S., Zou, Y., Cao, J., Wang, C., Hang, C., & Jin, L. (2023). Antioxidant and ammonia-sensitive films based on starch, κ-carrageenan and Oxalis triangularis extract as visual indicator of beef meat spoilage. *International Journal of Biological Macromolecules, 235*, Article 123698. https://doi.org/10.1016/j.ijbiomac.2023.123698

Jordheim, M., Giske, N. H., & Andersen, Ø. M. (2007). Anthocyanins in caprifoliaceae. *Biochemical Systematics and Ecology, 35*(3), 153–159. https://doi.org/10.1016/j.bse.2006.09.010

Juikar, S. K., & Warkar, S. G. (2023). Biopolymers for packaging applications: An overview. *Packaging Technology and Science, 36*(4), 229–251. https://doi.org/10.1002/pts.2707

Kalaycıoğlu, Z., Torlak, E., Akın-Evingür, G., Özen, İ., & Erim, F. B. (2017). Antimicrobial and physical properties of chitosan films incorporated with turmeric extract. *International Journal of Biological Macromolecules, 101*, 882–888. https://doi.org/10.1016/j.ijbiomac.2017.03.174

Kaya, M., Khadem, S., Cakmak, Y. S., Mujtaba, M., Ilk, S., Akyuz, L., Salaberria, A. M., Labidi, J., Abdulqadir, A. H., & Deligöz, E. (2018). Antioxidative and antimicrobial edible chitosan films blended with stem, leaf and seed extracts of Pistacia terebinthus for active food packaging. *RSC Advances, 8*(8), 3941–3950. https://doi.org/10.1039/c7ra12070b

Koosha, M., & Hamedi, S. (2019). Intelligent Chitosan/PVA nanocomposite films containing black carrot anthocyanin and bentonite nanoclays with improved mechanical, thermal and antibacterial properties. *Progress in Organic Coatings, 127*, 338–347. https://doi.org/10.1016/j.porgcoat.2018.11.028

Kossyvaki, D., Contardi, M., Athanassiou, A., & Fragouli, D. (2022). Colorimetric indicators based on anthocyanin polymer composites: A review. *Polymers, 14*(19), 4129. https://doi.org/10.3390/polym14194129

Kubota, N., & Eguchi, Y. (1997). Facile preparation of water-soluble N-acetylated chitosan and molecular weight dependence of its water-solubility. *Polymer Journal, 29*(2), 123–127. https://doi.org/10.1295/polymj.29.123

Kumar, D., Gihar, S., Shrivash, M. K., Kumar, P., & Kundu, P. P. (2020). A review on the synthesis of graft copolymers of chitosan and their potential applications. *International Journal of Biological Macromolecules, 163*, 2097–2112. https://doi.org/10.1016/j.ijbiomac.2020.09.060

Kurek, M., Hlupić, L., Ščetar, M., Bosiljkov, T., & Galić, K. (2019). Comparison of two pH responsive color changing bio-based films containing wasted fruit pomace as a source of colorants. *Journal of Food Science, 84*(9), 2490–2498. https://doi.org/10.1111/1750-3841.14716

Li, Y., Wu, K., Wang, B., & Li, X. (2021). Colorimetric indicator based on purple tomato anthocyanins and chitosan for application in intelligent packaging. *International Journal of Biological Macromolecules, 174*, 370–376. https://doi.org/10.1016/j.ijbiomac.2021.01.182

Liu, J., Liu, S., Wu, Q., Gu, Y., Kan, J., & Jin, C. (2017). Effect of protocatechuic acid incorporation on the physical, mechanical, structural and antioxidant properties of chitosan film. *Food Hydrocolloids, 73*, 90–100. https://doi.org/10.1016/j.foodhyd.2017.06.035

Mohamed, M. A., Marzouk, M. S. A., Moharram, F. A., El-Sayed, M. M., & Baiuomy, A. R. (2005). Phytochemical constituents and hepatoprotective activity of Viburnum tinus. *Phytochemistry, 66*(23), 2780–2786. https://doi.org/10.1016/j.phytochem.2005.07.019

Oladzadabbasabadi, N., Mohammadi Nafchi, A., Ariffin, F., Wijekoon, M. M. J. O., Al-Hassan, A. A., Dheyab, M. A., & Ghasemlou, M. (2022). Recent advances in extraction, modification, and application of chitosan in packaging industry. *Carbohydrate Polymers, 277*, Article 118876. https://doi.org/10.1016/j.carbpol.2021.118876

Pang, G., Zhou, C., Zhu, X., Chen, L., Guo, X., & Kang, T. (2023). Colorimetric indicator films developed by incorporating anthocyanins into chitosan-based matrices. *Journal of Food Safety, 43*(4), Article e13045. https://doi.org/10.1111/jfs.13045

Peh, K., Khan, T., & Ch'ng, H. (2000). Mechanical, bioadhesive strength and biological evaluations of chitosan films for wound dressing. *Journal of Pharmacy & Pharmaceutical Sciences, 3*(3), 303–311.

Pina, F., Alejo-Armijo, A., Clemente, A., Mendoza, J., Seco, A., Basílio, N., & Parola, A. J. (2021). Evolution of flavylium-based color systems in plants: What physical chemistry can tell us. *International Journal of Molecular Sciences, 22*(8), 3833. https://doi.org/10.3390/ijms22083833

Pina, F., Melo, M. J., Laia, C. A. T., Parola, A. J., & Lima, J. C. (2012). Chemistry and applications of flavylium compounds: A handful of colours. *Chemical Society Reviews, 41*(2), 869–908. https://doi.org/10.1039/C1CS15126F

Qin, Y., Wang, Y., Tang, Z., Chen, K., Wang, Z., Cheng, G., Chi, H., & Soteyome, T. (2024). A pH-sensitive film based on chitosan/gelatin and anthocyanin from Zingiber striolatum diels for monitoring fish freshness. *Food Chemistry: X, 23*(July), Article 101639. https://doi.org/10.1016/j.fochx.2024.101639

Shukla, R., Dubey, A., Pandey, V., Golhani, D., & Jain, A. P. (2012). Chromophore- An utility in UV spectrophotometer. *Inventi Rapid: Pharm Analysis & Quality Assurance, 2*(3), 1–4. *2012*.

Rojas-Bravo, M., Rojas-Zenteno, E. G., Hernández-Carranza, P., Ávila-Sosa, R., Aguilar-Sánchez, R., Ruiz-López, I. I., & Ochoa-Velasco, C. E. (2019). A potential application of mango (Mangifera indica L. cv Manila) peel powder to increase the total phenolic compounds and antioxidant capacity of edible films and coatings. *Food and Bioprocess Technology, 12*(9), 1584–1592. https://doi.org/10.1007/s11947-019-02317-8

Roy, S., & Rhim, J.-W. (2022). Genipin-crosslinked gelatin/chitosan-based functional films incorporated with rosemary essential oil and quercetin. *Materials, 15*(11), 3769. https://doi.org/10.3390/ma15113769

Roy, S., & Rhim, J. W. (2020). Preparation of carbohydrate-based functional composite films incorporated with curcumin. *Food Hydrocolloids, 98*(July 2019), Article 105302. https://doi.org/10.1016/j.foodhyd.2019.105302

Roy, S., & Rhim, J. W. (2021). Anthocyanin food colorant and its application in pH-responsive color change indicator films. *Critical Reviews in Food Science and Nutrition, 61*(14), 2297–2325. https://doi.org/10.1080/10408398.2020.1776211

Sahraee, S., Milani, J. M., Ghanbarzadeh, B., & Hamishehkar, H. (2017). Physicochemical and antifungal properties of bio-nanocomposite film based on gelatin-chitin nanoparticles. *International Journal of Biological Macromolecules, 97*(December), 373–381. https://doi.org/10.1016/j.ijbiomac.2016.12.066

Saravanakumar, K., Sathiyaseelan, A., Mariadoss, A. V. A., Xiaowen, H., & Wang, M. H. (2020). Physical and bioactivities of biopolymeric films incorporated with cellulose, sodium alginate and copper oxide nanoparticles for food packaging application. *International Journal of Biological Macromolecules, 153*, 207–214. https://doi.org/10.1016/j.ijbiomac.2020.02.250

Sever Yilmaz, B., Altun, M. L., Orhan, I. E., Ergene, B., & Saltan Citoglu, G. (2013). Enzyme inhibitory and antioxidant activities of *Viburnum tinus* L. relevant to its neuroprotective potential. *Food Chemistry, 141*(1), 582–588. https://doi.org/10.1016/j.foodchem.2013.03.020

Shankar, S., Khodaei, D., & Lacroix, M. (2021). Effect of chitosan/essential oils/silver nanoparticles composite films packaging and gamma irradiation on shelf life of strawberries. *Food Hydrocolloids, 117*, Article 106750. https://doi.org/10.1016/j.foodhyd.2021.106750

Sid, S., Mor, R. S., Kishore, A., & Sharanagat, V. S. (2021). Bio-sourced polymers as alternatives to conventional food packaging materials: A review. *Trends in Food Science and Technology, 115*, 87–104. https://doi.org/10.1016/j.tifs.2021.06.026

Siddiqui, N., Rauf, A., Latif, A., & Mahmood, Z. (2017). Spectrophotometric determination of the total phenolic content, spectral and fluorescence study of the herbal Unani drug Gul-e-Zoofa (Nepeta bracteata Benth). *Journal of Taibah University Medical Sciences, 12*(4), 360–363. https://doi.org/10.1016/j.jtumed.2016.11.006

Siripatrawan, U., & Harte, B. R. (2010). Physical properties and antioxidant activity of an active film from chitosan incorporated with green tea extract. *Food Hydrocolloids, 24*(8), 770–775. https://doi.org/10.1016/j.foodhyd.2010.04.003

Souza, V. G. L., Fernando, A. L., Pires, J. R. A., Rodrigues, P. F., Lopes, A. A. S., & Fernandes, F. M. B. (2017). Physical properties of chitosan films incorporated with natural antioxidants. *Industrial Crops and Products, 107*(February), 565–572. https://doi.org/10.1016/j.indcrop.2017.04.056

Stefanowska, K., Woźniak, M., Majka, J., Sip, A., Mrówczyńska, L., Kozak, W., Dobrucka, R., & Ratajczak, I. (2023). Chitosan films with caffeine and propolis as promising and ecofriendly packaging materials. *Applied Sciences, 13*(22), Article 12351. https://doi.org/10.3390/app132212351

Sutharsan, J., Boyer, C. A., & Zhao, J. (2022). Physicochemical properties of chitosan edible films incorporated with different classes of flavonoids. *Carbohydrate Polymer Technologies and Applications, 4*(June), Article 100232. https://doi.org/10.1016/j.carpta.2022.100232

Thakur, V. K., & Thakur, M. K. (2014). Recent advances in graft copolymerization and applications of chitosan: A review. *ACS Sustainable Chemistry and Engineering, 2*(12), 2637–2652. https://doi.org/10.1021/sc500634p

Wang, X., Yong, H., Gao, L., Li, L., Jin, M., & Liu, J. (2019). Preparation and characterization of antioxidant and pH-sensitive films based on chitosan and black soybean seed coat extract. *Food Hydrocolloids, 89*(August 2018), 56–66. https://doi.org/10.1016/j.foodhyd.2018.10.019

Wu, Y., Shi, Y., & Wang, H. (2023). Urea as a hydrogen bond producer for fabricating mechanically very strong hydrogels. *Macromolecules, 56*(12), 4491–4502. https://doi.org/10.1021/acs.macromol.3c00611

Xu, F., Liu, X., Tang, C., Yong, H., Kan, J., & Liu, J. (2025). Fabrication of chitosan/black rice anthocyanin composite films cross-linked with dialdehyde pullulan for shrimp freshness indicating. *Food Chemistry, 493*, Article 145716. https://doi.org/10.1016/j.foodchem.2025.145716

Yang, B., Liu, B., Gao, Y., Wei, J., Li, G., Zhang, H., Wang, L., & Hou, Z. (2024). PEG-crosslinked O-carboxymethyl chitosan films with degradability and antibacterial activity for food packaging. *Scientific Reports, 14*(1), Article 10825. https://doi.org/10.1038/s41598-024-61642-x

Yong, H., Wang, X., Bai, R., Miao, Z., Zhang, X., & Liu, J. (2019). Development of antioxidant and intelligent pH-sensing packaging films by incorporating purple-fleshed sweet potato extract into chitosan matrix. *Food Hydrocolloids, 90*, 216–224. https://doi.org/10.1016/j.foodhyd.2018.12.015

Zhang, W., & Jiang, W. (2020). Antioxidant and antibacterial chitosan film with tea polyphenols-mediated green synthesis silver nanoparticle via a novel one-pot method. *International Journal of Biological Macromolecules, 155*, 1252–1261. https://doi.org/10.1016/j.ijbiomac.2019.11.093

Zhang, X., Liu, Y., Yong, H., Qin, Y., Liu, J., & Liu, J. (2019). Development of multifunctional food packaging films based on chitosan, TiO2 nanoparticles and anthocyanin-rich black plum peel extract. *Food Hydrocolloids, 94*, 80–92. https://doi.org/10.1016/j.foodhyd.2019.03.009